Received: 18 October 2018 | Revised: 5 March 2019 | Accepted: 16 May 2019
DOI: 10.1002/we.2377

WILEY

RESEARCH ARTICLE

Low-frequency dynamics of a floating wind turbine in wave tank–scaled experiments with SiL hybrid method

José Azcona | Faisal Bouchotrouch | Felipe Vittori

Wind Energy Department, Centro Nacional de Energías Renovables, CENER, Sarriguren, Spain

Correspondence
José Azcona Armendáriz, Wind Energy Department, Ciudad de la Innovación 7, CENER, Sarriguren 31621, Navarra, Spain.
Email: jazcona@cener.com

Present Address
CENER, Ciudad de la Innovación 7, 31621 Sarriguren, Navarra, Spain.

Funding information
FP7 Energy, Grant/Award Number: 308974; FP7 Research infrastructures, Grant/Award Number: 262552

Abstract

The design of floating wind turbines needs the validation of numerical models against measurements obtained from experiments that accurately represent the system dynamics. This requires solving the conflict in the scaling of the hydrodynamic and aerodynamic forces that arises in tests with wind and waves. To sort out this conflict, we propose a hybrid testing method that uses a ducted fan to replace the rotor and introduce a force representing the aerodynamic thrust. The force is obtained from a simulation of the rotor coupled in real time with the measured platform displacements at the basin. This method is applied on a test campaign of a semisubmersible wind turbine with a scale factor of 1/45. The experimental data are compared with numerical computations using linear and non-linear hydrodynamic models. Pitch decays in constant wind show a good agreement with computations, demonstrating that the hybrid testing method correctly introduces the aerodynamic damping. Test cases with constant wind and irregular waves show better agreement with the simulations in the power spectral density's (PSD's) low-frequency region when non-linear hydrodynamics are computed. In cases with turbulent wind at rated wind speed, the low-frequency platform motions are dominated by the wind, hiding the differences from hydrodynamic non-linearities. In these conditions, the agreement between experiments using the proposed hybrid method and computations is good in all the frequency range both for the linear and the non-linear hydrodynamic models. Conversely, for turbulent winds producing lower rotor thrust, non-linear hydrodynamics are relevant for the simulation of the low-frequency system dynamics.

KEYWORDS

aerodynamics, floating wind turbine, hybrid testing, hydrodynamics, integrated codes, non-linear hydrodynamics, wave tank

1 | INTRODUCTION

Floating platforms allow wind turbines operating at high water depths unlocking a great energy potential in vast sea areas. The development of this technology has been accelerating in recent years, with several successful projects currently at prototype stage. In 2017, the first offshore floating wind farm, the Hywind project, in Scotland, started delivering power to the grid.

Scaled wave tank testing is an important step for the validation of a concept during the design process. The relevant forces acting on the system, their frequencies, the masses and the inertias have to be accurately scaled to achieve reliable conclusions on the full-scale dynamic behaviour of the concept tested. The common practice in these tests is to base the scaling on the Froude number, to ensure the similarity of the hydrodynamic forces.[1] Unfortunately, with this method, the resulting Reynolds number that determines the aerodynamic loads on the blade airfoils is lower than in full scale and, in consequence, the resulting forces on the rotor are out of scale.[2] Several methods have been proposed to overcome this scaling conflict and obtain representative aerodynamic forces on the rotor during the scaled experiments, such as redesigning the scaled rotor for a low Reynolds condition[3] or using a tuned drag disk instead of the scaled rotor.[4] An alternative approach is the real-time hybrid testing, where the aerodynamic rotor thrust on the wind turbine is applied based on simultaneous simulations (coupled to the experiments), while the waves and the floater response are physically tested. We first proposed and validated a hybrid testing method for floating

wind turbine–scaled tests combining wind and waves in 2014, and we called it software in the loop (SiL).[2] In our setup, a ducted fan is used to apply the force representing the total rotor thrust that is computed in real time by a numerical model. Other hybrid methods are discussed in Chabaud et al[5] and Hall et al.[6] Recently, wires have been used to introduce the rotor thrust in hybrid test campaigns for horizontal axis wind turbines in Bachynski et al[7] and Hall and Goupee[8] and for vertical axis wind turbines.[9] An effort to define the specifications and requirements of hybrid testing methods has been carried out in Hall et al[10] and Müller et al.[11] The importance of non-linear hydrodynamics and wind loading in the low-frequency dynamics of floating wind turbine has been studied in previous publications. Nevertheless, there is a lack of comparisons between experimental measurements and equivalent numerical simulations combining wind and waves. The work presented in Bayati et al[12] uses numerical models of a semisubmersible wind turbine to conclude that non-linear effects cannot be neglected to accurately capture the system dynamics. Nevertheless, the effect of wind loading is not investigated, and no comparisons with test measurements are presented. In Duarte et al,[13] the influence of second-order hydrodynamic forces on the low-frequency dynamics of a spar is studied numerically. This work includes the effect of wind, but the numerical results are not compared with experimental measurements. It concludes that both the rotor thrust and the second-order hydrodynamics can play a role in the spar's low-frequency dynamics. In Coulling et al,[14] the importance of second-order difference frequency forces on a semisubmersible floating wind turbine is discussed in comparison with the effect of the wind loading. The conclusions obtained from numerical analysis of combined wind and wave simulations are supported by the trends observed on the DeepCwind test campaign,[15] although no comparison is done between measurements and computations. The aerodynamic forces in the DeepCwind test campaign were included using a Froude-scaled wind turbine, instead of a hybrid approach to circumvent the conflict in the scaling of aerodynamic and hydrodynamic forces. They conclude that it is reasonable to exclude second-order hydrodynamics for floating wind turbines in production because the aerodynamic thrust dominates the low-frequency dynamics but they should be included when the rotor thrust is lower such as in parked/idling condition. More recently, experimental results of a floating wind turbine using a hybrid approach with wires to introduce the rotor thrust have been presented in Thys et al,[16] although the measurements are not compared with numerical simulations and second-order hydrodynamic effects are not discussed. They show that the wind turbulence plays a role on the low-frequency dynamics of the platform.

The present work discusses the relative importance of the second-order hydrodynamic forces and the wind loads in the floating wind turbine low-frequency dynamics with an approach both numerical and experimental, covering a gap in previous works. The experimental results of the floating wind turbine are obtained using a hybrid approach for the correct scaling of the aerodynamic loads. The numerical model allows enabling and disabling the second-order effects of the hydrodynamic model to assess their importance compared with the wind load. The comparisons between simulations and measurements validate the conclusions for the semisubmersible platform.

2 | SiL METHOD

The method consists of a ducted fan installed in the scaled model at the hub height instead of the rotor. This fan is driven by an electric motor and introduces a force during the test to represent the aerodynamic rotor force. This force is controlled through the fan rotational speed set by the controller, which again depends on a real-time simulation that computes the rotor thrust. This numerical simulation runs simultaneously with the tests and considers the platform motions measured in real time in the wave tank. Thus, the system emulates the rotor aerodynamic damping that has an important impact on the global system dynamics. The rotor simulation also includes the control strategy and can consider different operating regimes of the wind turbine (power, production, idling and stops) or different wind conditions (turbulent wind, constant wind and gusts). This method is cost efficient; the required materials are not expensive and can be recycled for future campaigns, as they are not

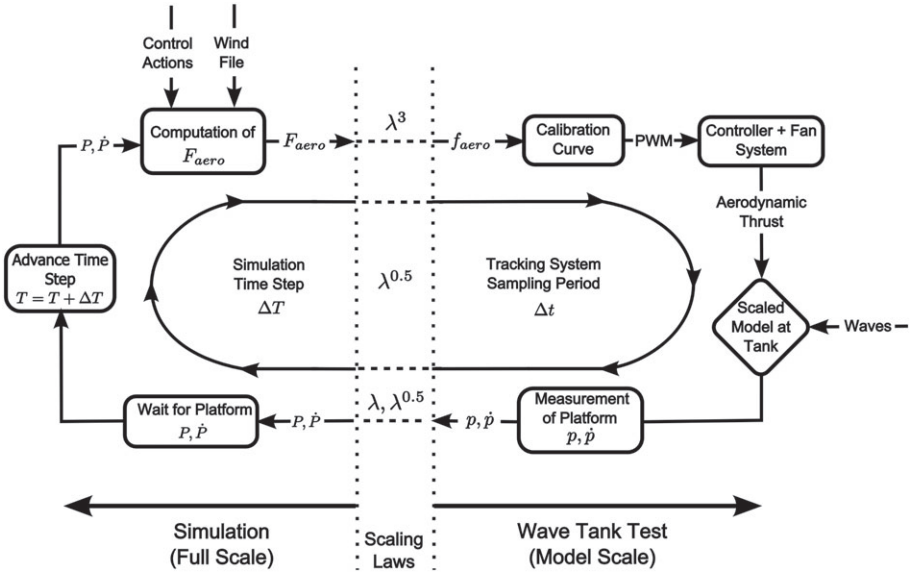

FIGURE 1 Diagram of the Software-in-the-Loop method

specific for a certain wind turbine design. Currently, the method introduces the rotor force in a single point, and therefore, it does not match the gyroscopic momentum or the aerodynamic torque. Although these effects have less influence on the global dynamics of floating wind turbines, we plan to include them in future test campaigns.

Figure 1 presents a flowchart with the basic layout of the SiL method. The left side of the diagram describes the full-scale numerical simulation, and the right side represents the wave tank–scaled test. The different magnitudes that are interchanged are transformed by the appropriate scaling laws based on the factor scale λ. The numerical simulation provides the total aerodynamic force on the shaft, F_{aero}, from integration of the aerodynamic loads computed at the blade elements. This force, calculated in full scale, is transformed to the model scale (f_{aero}). A calibration curve provides the width of the pulse width modulation (PWM) signal that is sent to the controller to modulate the fan speed in order to achieve the desired force at the model's rotor position. At the same time, the wave maker is generating waves that, together with the aerodynamic thrust, induce the platform motions. The motions are measured by the optical motion tracking system for the 6 degrees of freedom of the platform (three translations and three rotations) at a certain sampling period, Δt. The measurements are sent to the numerical model that is waiting for the data to advance one time step, ΔT, in the integration scheme and update the aerodynamic thrust. The sampling period of the motion tracking system, Δt, and the simulation time step, ΔT, must be related by the time scaling factor of $\lambda^{0.5}$.

3 | FLOATING WIND TURBINE MODEL

The floating wind turbine used in this work is based on the geometry, mass distribution, and inertias of the OC4 DeepCwind semisubmersible specified in Robertson et al.[17] The platform supports the NREL 5-MW wind turbine,[18] which is a three bladed upwind horizontal axis wind turbine with a hub height of 90 m and a rotor radius of 126 m. On the basis of these specifications, a physical scaled model was built to be tested at the wave tank, and a numerical model of the rotor was developed to compute the rotor thrust to be introduced during the tests using the SiL methodology. In addition, a numerical model of the complete wind turbine and platform was built to generate numerical results to be compared with the experimental measurements and obtain the conclusions that are drawn at the end of this paper.

3.1 | Scaled model used in the experiments

The test campaign was performed at the École Centrale de Nantes (France) using a 1/45 scaled model of the OC4 DeepCwind floating wind turbine model. Figure 2 shows the scaled model at the wave tank, with one column situated upwind and two columns downwind. The reference system used to represent the platform motions is shown. The system's origin is located at the still water level (SWL) and at the tower centre axis. The *x*-axis is oriented in the nominal downwind direction, the *z*-axis is oriented upwards, and the *y*-axis is oriented to the left when looking downwind. The nominal wave direction is parallel to the *x*-axis.

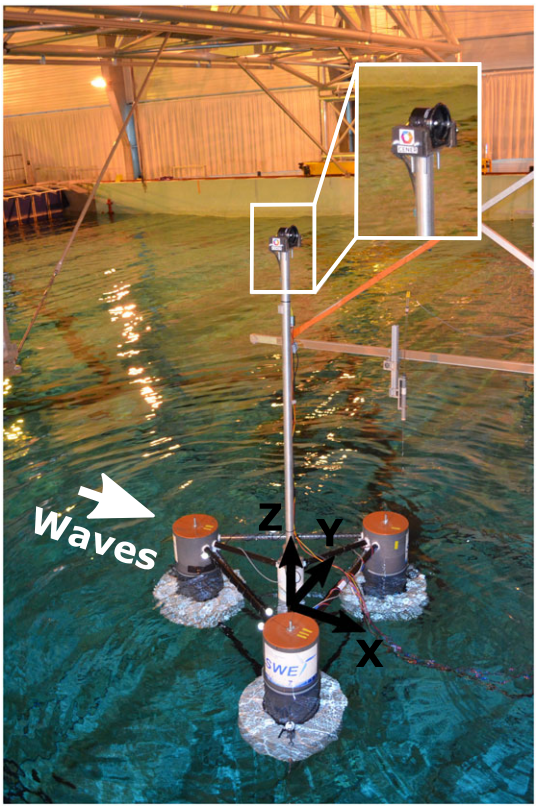

FIGURE 2 OC4 DeepCwind semisubmersible scaled model at the wave tank and reference system [Colour figure can be viewed at wileyonlinelibrary.com]

Figure 2 also shows the ducted fan mounted at the tower top. The mass of the ducted fan is relatively low, and ballast was added at the tower top to match the target mass representing the full-scale rotor nacelle assembly (RNA). Once the construction of the scaled floating wind turbine model was finished, the properties of the system were measured by means of pendulum and inertia tests to characterize the resulting properties. The main properties for the global system without mooring lines (ducted fan, tower top ballast, tower and platform) are presented in full scale in Table 1. The inertias are presented around the global system centre of mass (CM).

The nominal water depth of the wave tank is 5 m, but during the test campaign, it was detected a slight decrease of the water depth to 4.958 m. In consequence, we assumed a full-scale water depth of 223.11 m. The original dimensions of the mooring system[17] had to be truncated to accommodate it to the wave tank dimensions. The mooring system is composed of three lines with an angle of 120° between them and with one line upwind (line 2) and two lines downwind (line 1 and line 3). A DIN 763 chain with 2 mm of wire diameter was used to represent the lines in the basin. Table 2 presents the full-scale properties of the mooring system installed within the basin.

For the integration of the SiL method during the tests, the LabVIEW software was used to acquire the data from the wave tank motion tracking system (Qualisys) and to communicate with the wind turbine simulation software during the test execution. A TCP/IP network protocol was selected for the communication between LabVIEW and Qualisys and also between LabVIEW and the simulation code.

The ducted fan model selected to generate the force representing the aerodynamic thrust is the DS-30-AXI HDS, manufactured by the German company Schübeler. As shown in Figure 3, the fan is powered by a brushless motor, model HET 2W20, that is controlled by an electronic speed controller (ESC) YGE 90 HV and works with an industrial alternating current (AC)/direct current (DC) power supply. This system configuration produces an approximate force range of 0 to 18 N. The revolutions per minute (rpm) of the motor (and therefore the force produced by the fan) is controlled by a PWM signal generated with the LabVIEW control software, using servo libraries for Arduino. The demanded force for the fan is provided by the full-scale simulation of the rotor aerodynamic thrust. During the calibration of the ducted fan, we performed step change tests confirming that the dynamic response of the fan was similar to the behaviour of the fan system used succesfully in previous test campaign.[2] Nevertheless, due to time constraints, we were not able to perform a systematic analysis of the frequency response of the system, which is an aspect that we plan to investigate in detail in the future.

A numerical model of the NREL 5-MW wind turbine[18] was built to compute the aerodynamic loads in real time during the tests. The FAST code[19] version v6.02c-jmj coupled with AeroDyn version 12.58 was used. This code is widely used in the sector and, in contrast with other commercial codes, is an open-source software that can be modified. The code was adapted for the requirements of the SiL method, computing the thrust in real time during the tests, coupled with the wave tank's motion tracking system. In addition, the software is based on blade element momentum (BEM) theory, which is a numerical model for the rotor's aerodynamic computation with a high computational efficiency in

TABLE 1 Platform main properties

System CM vertical position below SWL, m	9.63
System mass including water ballast, kg	$1.39\ 10^7$
System inertia in roll around CM, kgm^2	$1.22\ 10^{10}$
System inertia in pitch around CM, kgm^2	$1.22\ 10^{10}$
System inertia in yaw around CM, kgm^2	$1.15\ 10^{10}$
Platform-displaced volume, m^3	14 245.0

Abbreviations: CM, centre of mass; SWL, still water level.

TABLE 2 Description of the mooring system at the wave tank

Anchor radial distance from undisplaced platform centre, m	769.65
Anchor depth location, m	223.1
Fairlead radial distance from platform centre, m	41.76
Fairlead draft from still water level (SWL), m	15.03
Unstretched line 1 length, m	777.28
Unstretched line 2 length, m	777.24
Unstretched line 3 length, m	777.15

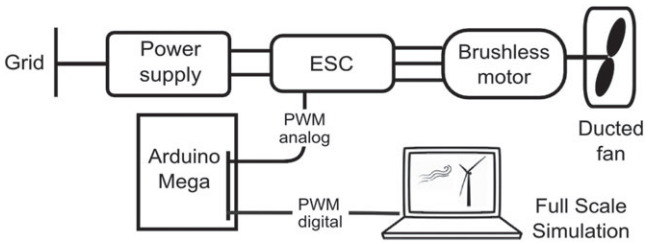

FIGURE 3 Fan control system layout

comparison with more complex solutions. The low central processing unit (CPU) cost is an important constraint in hybrid testing methods with real-time simulations. The software was compiled in Linux, and it was run on a computer with a 2.54-GHz Intel Core Duo CPU and 2 GB of RAM.

The AeroDyn code is based on the BEM theory, and the Glauert correction was included for the computation of the rotor thrust. The tip and hub losses were also considered through the Prandtl correction. The blades and the tower were assumed rigid in the numerical model. No drag loads nor aerodynamic effects were included for the tower. The turbulent wind files were generated with TurbSim version 1.50[20] using Kaimal spectrum. The conventional variable rotor speed and variable blade pitch control strategy for the wind turbine described in Robertson et al[17] was used.

3.2 | Numerical model for simulations

A numerical model of the floating wind turbine tested in the wave tank was built at full scale to obtain the comparisons between numerical results and measurements that will be shown in the next section. The model was built in FAST version 8 based on the system properties from Table 1. The frequency domain hydrodynamic properties of the platform were computed using the WAMIT panel code.[21] A first version of the model was developed based on potential linear theory for the representation of the floater's hydrodynamics. A second version of the model was built including non-linear hydrodynamics by means of the quadratic transfer functions (QTFs) of the platform. These QTFs are also calculated with WAMIT and allow computing the second-order wave excitation loads that can be linearly superimposed with the first-order loads (see, for example, Duarte et al[13]). The inclusion of QTFs requires an important computational effort, increasing the CPU cost around three times. The numerical model assumed a water density of 999 kg/m^3, representative of the sweet water at the wave tank.

Viscous damping and excitation based on the relative form of Morison formulation were applied to the slender members of the platform. According to Robertson et al,[17] different values for the drag coefficient were applied to the central column (0.56), the upper external columns (0.61), the base external columns (0.68), the pontoons and cross member (0.63) and the heave plate (4.8).

Free decay tests were used to tune the damping of the numerical model, increasing linear damping and quadratic damping in surge (2.0 10^4 Ns/m and 8.0 10^5 Ns^2/m^2, respectively) and linear damping in pitch (3.0 10^8 Nms/rad). An additional stiffness of 5.0 10^3 N/m was also added in surge to take into account the effect of the cabling during the tests.

The aerodynamic model of the NREL 5-MW baseline wind turbine was built in AeroDyn version 14. For consistency, it was defined a similar configuration of the AeroDyn model that was used within the SiL scheme for the computation of the rotor thrust during the tank tests. Therefore, the Glauert correction and the tip and hub losses using the Prandtl correction were implemented in the numerical model. The blades and the tower were also considered rigid. In addition, the same controller and the same wind files used during the SiL computations for the tests were used in the subsequent numerical simulations for comparison. The wave elevation time series measured during the test cases were used to generate the wave kinematics during the equivalent numerical simulations.

A numerical model of the mooring system, according to the geometry described in Table 2 was built using MoorDyn,[22] which is a simulation code for mooring line dynamics that is coupled with FAST version 8. The volume of water displaced by the DIN 763 chain that represents the scaled mooring lines was measured, and the resulting equivalent diameter, used by the numerical model to calculate the buoyancy of the line, was 3.18 mm (143.0 mm in full scale). The weight of the chain was also measured, resulting in a value of 125.5 kg/m in full scale. The axial stiffness was set to 7.536 10^8 N, as reported by the OC4 DeepCwind floating wind turbine description.[17] According to DNV,[23] the normal and tangential drag coefficients of the lines were set to 2.4 and 1.1, respectively. The added mass coefficient was set to 1.0.[24]

4 | COMPARISON BETWEEN MEASUREMENTS AND SIMULATIONS

This section presents the comparisons between the experimental measurements and the numerical simulation results of equivalent cases. All the results are shown in full scale in the reference system represented in Figure 2. The cases discussed are presented in order of increasing complexity: first, platform pitch decays with constant wind, then irregular waves with constant wind and finally combined cases with irregular waves and turbulent winds.

4.1 | Decay tests in constant wind

Pitch decay tests under constant wind were performed using the SiL system to introduce the coupled aerodynamic rotor thrust. The SiL computation included the effect of the controller and also the variation of the relative wind speed induced by the pitch motion of the platform.

The experiment was performed for three wind speeds: 8.5 m/s (below rated wind speed), 11.4 m/s (rated wind speed) and 18 m/s (above rated wind speed), covering the different control regions. The measured pitch for the different wind speeds is compared with equivalent simulations in Figure 4. Additionally, a comparison between the measured and the computed free decay with no wind is included on the top of the figure for reference. This pitch-free decay signal was used, together with other pitch-free decays from the test campaign, to tune the linear pitch damping that was included in the numerical model, as mentioned in Subsection 3.2. The natural periods and damping ratios extracted from the signals in Figure 4 are gathered in Table 3, to allow a better comparison.

For the three wind speeds considered, the pitch decays including constant wind present higher damping ratios than the reference-free decay with no wind loading. The 11.4 m/s wind speed produces the highest rotor thrust and the highest damping ratio (0.15). The decay tests at 8.5 and

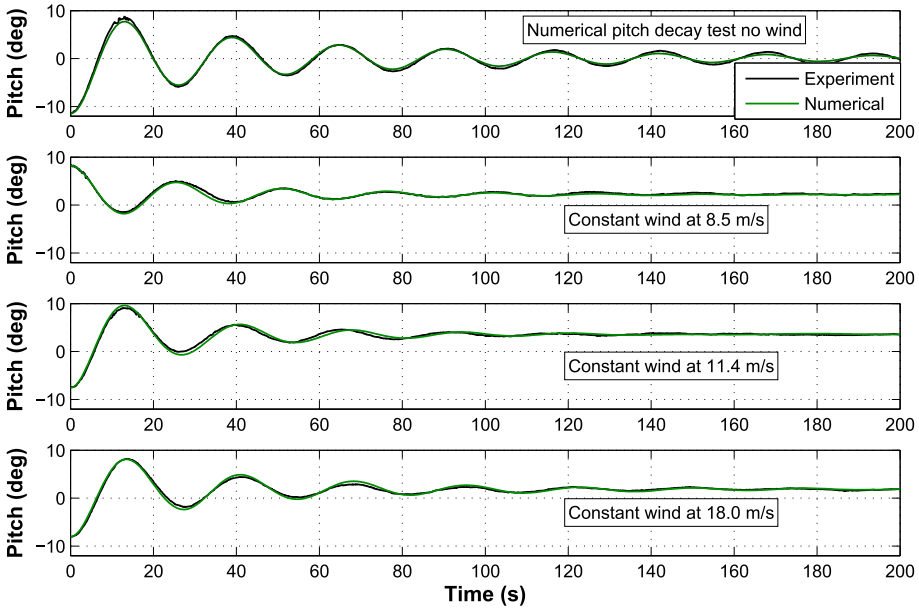

FIGURE 4 Pitch-free decay test and pitch decay tests in constant wind [Colour figure can be viewed at wileyonlinelibrary.com]

TABLE 3 Natural periods and damping ratios of the pitch decay tests

	Natural Period (s)		Damping Ratio (–)	
Wind Speed (m/s)	Experimental	Numerical	Experimental	Numerical
No. aerodynamic loading	26.16	25.95	0.094	0.099
8.5	25.62	25.50	0.123	0.126
11.4	26.80	27.10	0.150	0.150
18	27.23	27.35	0.136	0.123

18 m/s present lower damping ratios, but they are still higher than for the case with no wind. The periods computed with numerical tools are very close to the measured periods from the experiments, with maximum differences around 1.1%. The numerically predicted damping ratio for the reference case with no wind presents a difference around 6% with the damping ratio from the equivalent measured decay. When the constant wind is added, damping ratios from simulated and measured decays agree very well for 8.5 m/s and 11.4 m/s wind speeds (differences of 2.5% and 0.3%, respectively). For the case with 18 m/s wind speed, the difference between the damping ratio from numerical and experimental results is around 9%.

4.2 | Constant wind and irregular waves

The measurements performed during two test cases with constant wind and irregular waves are compared in this section against simulations. Constant wind provides no wind loading in the low-frequency region of the power spectral density (PSD) plots. This allows to evaluate the level of agreement of linear and non-linear hydrodynamic models and the experimental measurements in this region.

In the first case, the sea state follows a JONSWAP spectrum with significant wave height $H_s = 4.13$ m and spectral peak period $T_p = 7.3$ seconds, and the constant wind speed is 11.4 m/s in full scale. The second case considers a significant wave height $H_s = 4.88$ m, a spectral peak period $T_p = 8.9$ seconds, and a constant wind speed of 18 m/s. Two simulations for each case have been launched: one with a linear potential hydrodynamic model and another one including the full sum and difference frequency QTFs.

For the first case considered, Figures 5 and 6 present the PSDs of the measured and the computed surge and pitch responses of the platform. Similarly, for the second case, Figures 7 and 8 compare the experimental measurements and the computations for the surge and pitch degrees of freedom.

In both cases, the agreement between the experimental and the numerical surge and pitch motions is good in the linear region, around the wave peak period (0.137 Hz for the first case and 0.112 Hz for the second one), with independence of the hydrodynamic model used in the computations. At lower frequencies, the non-linear difference frequency wave forces play an important role in the platform dynamics, because they excite the surge natural frequency (0.008 Hz) and the pitch natural frequency (0.037 Hz). In consequence, the numerical solution using linear hydrodynamics underpredicts the response for both surge and pitch in the low-frequency region. If the effect of full QTF is included in the simulation, the numerical results match better the experiments, although they still underpredict the wave tank measurements at the low-frequency region.

Finally, it has to be pointed out that the experimental pitch motion presents higher excitation at high frequencies than the numerical models. It has to be investigated if this is caused by spurious high-frequency noise from the ducted fan.

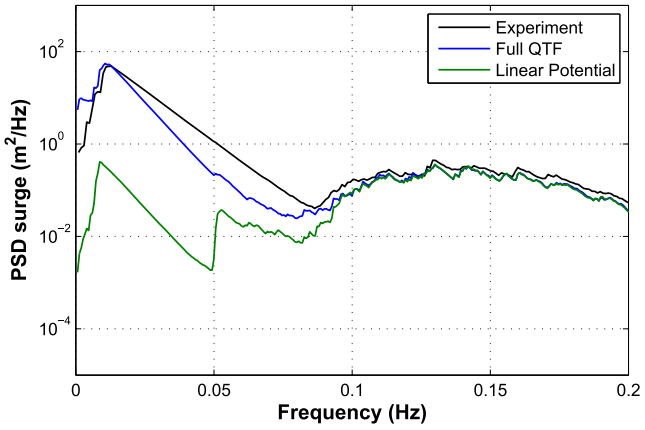

FIGURE 5 Surge power spectral density (PSD). Irregular waves ($H_s = 4.13$ m, $T_p = 7.3$ s) and constant wind (11.4 m/s) [Colour figure can be viewed at wileyonlinelibrary.com]

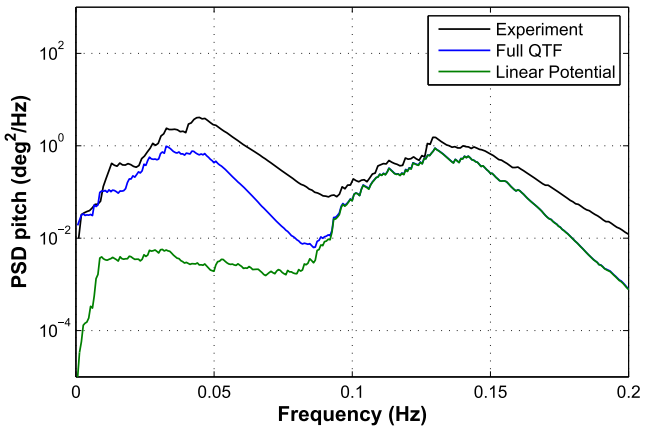

FIGURE 6 Pitch power spectral density (PSD). Irregular waves ($H_s = 4.13$ m, $T_p = 7.3$ s) and constant wind (11.4 m/s) [Colour figure can be viewed at wileyonlinelibrary.com]

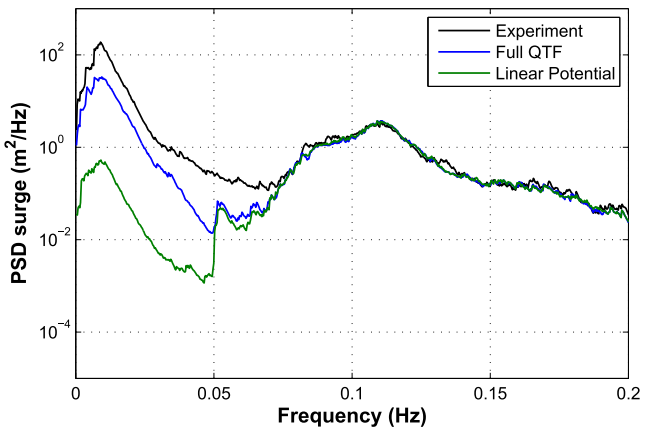

FIGURE 7 Surge power spectral density (PSD). Irregular waves ($H_s = 4.88$ m, $T_p = 8.9$ s) and constant wind (18 m/s) [Colour figure can be viewed at wileyonlinelibrary.com]

4.3 | Turbulent wind and irregular waves

In this section, two cases with turbulent wind and irregular waves are compared with simulations. To obtain a better consistency between the computations and the measurements at the wave tank, the same turbulent wind files that were used in the SiL computations are used for the simulation of the equivalent cases. Also, the wave elevation time series measured for each test case at the tank were used to generate the wave kinematics in full scale for the equivalent simulation. The definition of the conditions for these cases is similar to the ones discussed in the previous Subsection 4.2 (the same sea states are used), but instead of a constant wind, a turbulent wind is defined with the same mean speed. In contrast to constant winds, turbulent winds introduce loading in the low-frequency region of the PSDs.

In the first case considered, the floating wind turbine experiments a turbulent wind with 11.4 m/s mean speed that follows a Kaimal spectrum with 19.89% turbulence intensity. The sea state is represented by a JONSWAP spectrum with significant wave height $H_s = 4.13$ m and spectral peak period $T_p = 7.3$ seconds. Figures 9 and 10 compare the PSD for the measured and the computed surge and pitch displacements.

Measured surge motions in Figure 9 agree very well with numerical simulations in all the frequency range, in particular for the surge natural frequency (0.008 Hz) and around the wave spectral peak frequency (0.137 Hz). For the pitch motion, in Figure 10, the agreement is also very

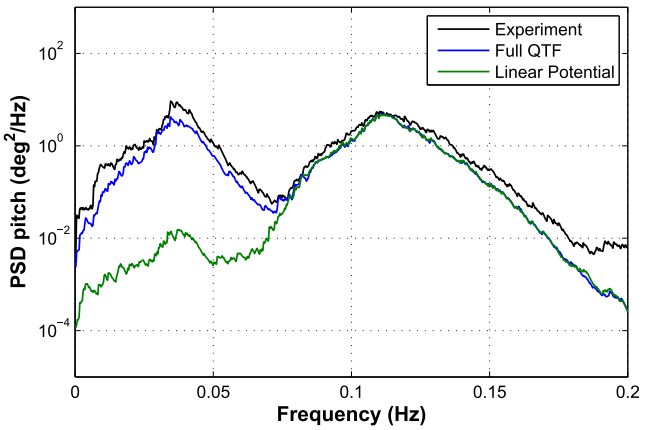

FIGURE 8 Pitch power spectral density (PSD). Irregular waves (H_s = 4.88 m, T_p = 8.9 s) and constant wind (18 m/s) [Colour figure can be viewed at wileyonlinelibrary.com]

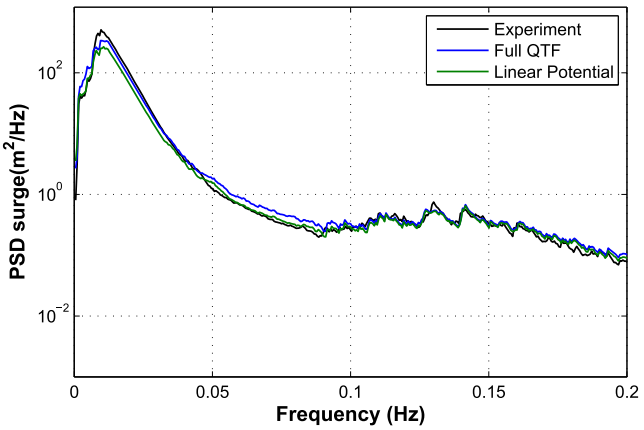

FIGURE 9 Surge power spectral density (PSD). Irregular waves (H_s = 4.13 m, T_p = 7.3 s) and turbulent wind (V_{mean} = 11.4 m/s) [Colour figure can be viewed at wileyonlinelibrary.com]

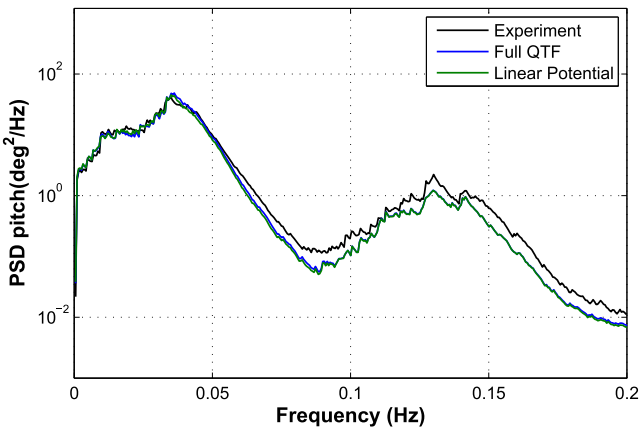

FIGURE 10 Pitch power spectral density (PSD). Irregular waves (H_s = 4.13 m, T_p = 7.3 s) and turbulent wind (V_{mean} = 11.4 m/s) [Colour figure can be viewed at wileyonlinelibrary.com]

good at low frequencies, around the pitch natural frequency (0.037 Hz), although for the wave peak frequency region, the numerical models slightly underpredict the measured pitch motion.

The rated mean wind speed (11.4 m/s) produces the highest thrust on the rotor. As the turbulent wind loading is a low-frequency excitation, the rotor aerodynamic thrust governs the platform surge and pitch motions in this region of the PSD. For this reason, the differences that were observed with constant wind in the low-frequency region caused by non-linear hydrodynamics (Figures 5 and 6) are hidden by the turbulent wind excitation. With turbulent wind, both linear and non-linear hydrodynamic models provide very similar results not only on the linear loading region but also at the low-frequency region.

Figure 11 displays a time domain comparison of the measured and computed platform pitch motion for this case. The plot illustrates how the experimental results obtained with the SiL method can be accurately reproduced in time domain by the numerical model. In addition, Figure 12 compares, for illustration purposes, the computed blade pitch angle in the SiL simulation during the experiment with the blade pitch angle obtained from pure simulations. The pitch activity in the SiL computations and in the totally numerical simulations is very similar.

The second case consists of a turbulent wind of 18 m/s mean speed with 17.0% turbulence, based on Kaimal spectrum, and a JONSWAP sea state with H_s = 4.88 m and T_p = 8.9 seconds. The wind turbine operates in the pitch control region, and the aerodynamic thrust is lower than for the previous case at rated mean wind speed. As the relative importance of the aerodynamic thrust on the system dynamics decreases, the

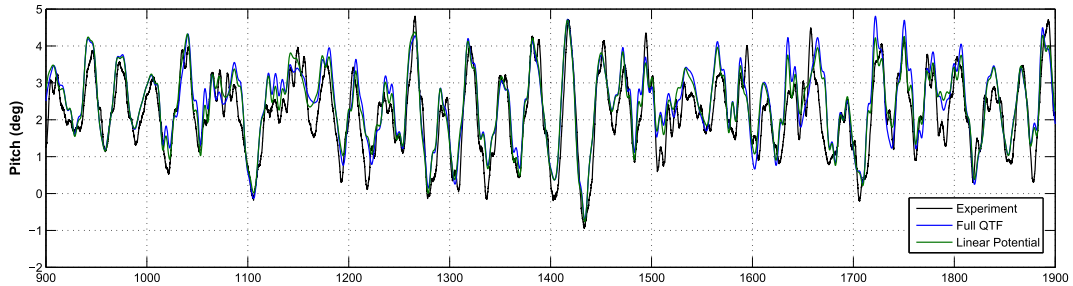

FIGURE 11 Time domain pitch motion. Irregular waves ($H_s = 4.13$ m, $T_p = 7.3$ s) and turbulent wind ($V_{mean} = 11.4$ m/s) [Colour figure can be viewed at wileyonlinelibrary.com]

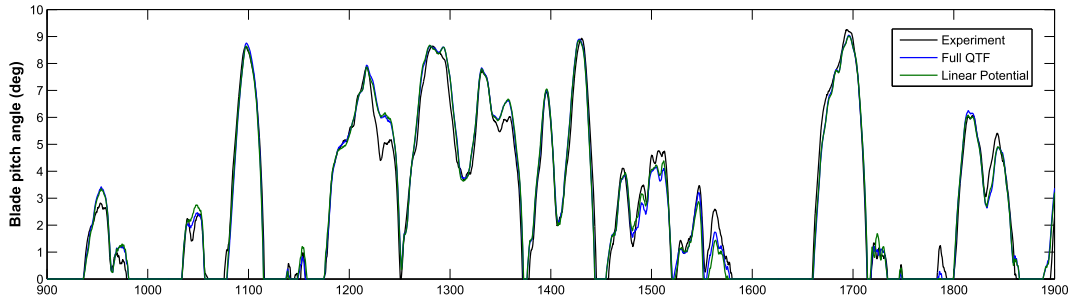

FIGURE 12 Time domain blade pitch angle. Irregular waves ($H_s = 4.13$ m, $T_p = 7.3$ s) and turbulent wind ($V_{mean} = 11.4$ m/s) [Colour figure can be viewed at wileyonlinelibrary.com]

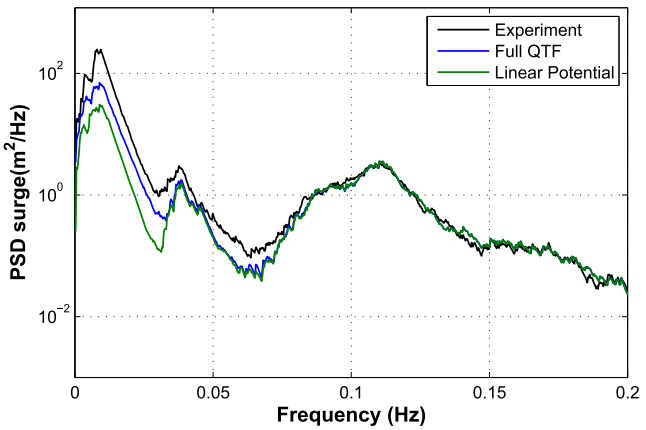

FIGURE 13 Surge power spectral density (PSD). Irregular waves ($H_s = 4.88$ m, $T_p = 8.9$ s) and turbulent wind ($V_{mean} = 18$ m/s) [Colour figure can be viewed at wileyonlinelibrary.com]

differences between the two hydrodynamic models arise when the PSD for the experimental and numerical surge displacement is compared in Figure 13. The plot shows that for the low-frequency region, the linear hydrodynamic model gives a lower surge than the full QTF response, with a better match to the experimental data. In the linear wave loading region of the PSD, around the wave peak frequency, both numerical models match very well the measurements.

Figure 14 represents the PSD for the experimental and numerical platform pitch motion. In contrast with surge, the role of non-linear hydrodynamics for the pitch motion is not relevant for these conditions, and both models agree well with the measurements. The pitch motion is still dominated by the rotor loading and the differences coming from the hydrodynamic model are hidden by this effect. This contrasts with the case with the same wave condition but with constant wind (Figures 7 and 8) where not only the surge but also the pitch motion was very dependant of the hydrodynamic model in the absence of turbulent wind.

It has been shown that for the case at rated wind speed, the rotor thrust hides the differences in the platform surge motion coming from the inclusion of hydrodynamic non-linearities (Figure 9). For the case with 18 m/s mean wind speed, the rotor thrust decreases, and differences from non-linear hydrodynamics arise in the surge motion (Figure 13). To better illustrate this aspect, Figure 15 compares the PSD of the rotor thrust and the non-linear hydrodynamic force obtained from the QTFs for both cases. For the first case, with 11.4 m/s mean wind speed, the aerodynamic thrust is about twice the non-linear hydrodynamic force. In contrast, for the case at 18 m/s, the aerodynamic force is on the range of the non-linear hydrodynamic force.

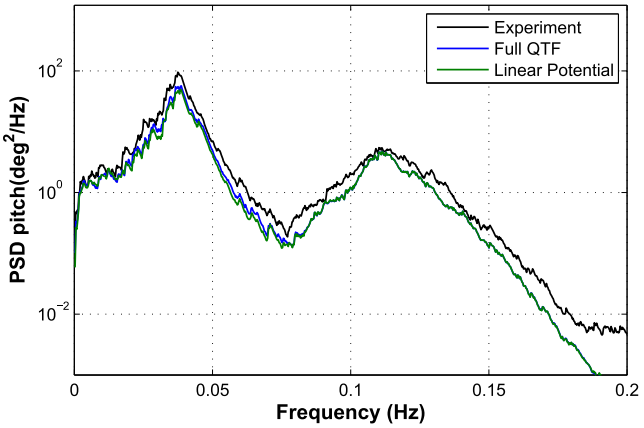

FIGURE 14 Pitch power spectral density (PSD). Irregular waves ($H_s = 4.88$ m, $T_p = 8.9$ s) and turbulent wind ($V_{mean} = 18$ m/s) [Colour figure can be viewed at wileyonlinelibrary.com]

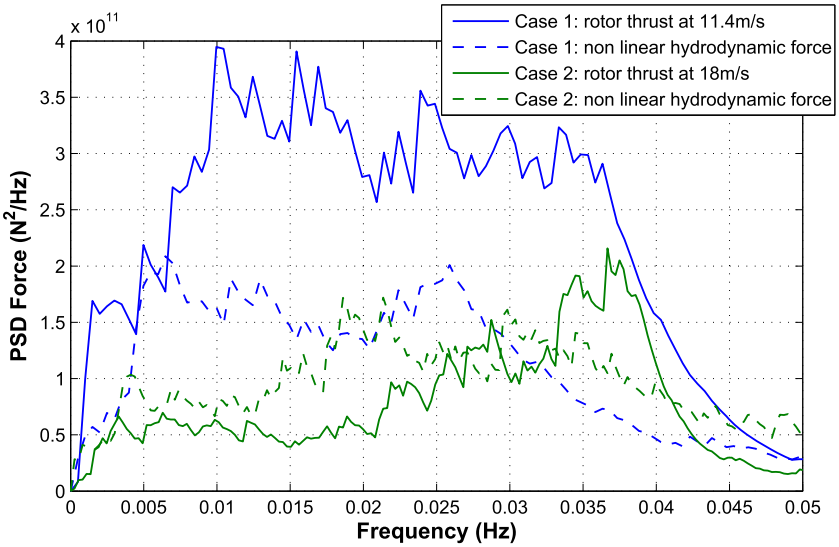

FIGURE 15 Power spectral densities (PSDs) of the rotor thrust and the non-linear hydrodynamic force for the two cases considered [Colour figure can be viewed at wileyonlinelibrary.com]

5 | CONCLUSIONS

The SiL hybrid testing method was applied for the integration of the coupled wind loading during a scaled wave tank test campaign of the 5 MW OC4 DeepCwind semisubmersible floating wind turbine. The experimental data were compared with numerical computations using linear and non-linear full QTF hydrodynamic models.

The platform pitch decays show an increase in damping when a constant wind is included, compared with the case without wind loading. The pitch decays with three different constant wind speeds agree well with the equivalent numerical simulations in frequency and damping ratio, although at 18 m/s, the difference in damping is slightly higher. This demonstrates the performance of the SiL method to introduce, based on a coupled computation, the aerodynamic damping in scaled tests, which is a relevant effect in the global dynamics of floating wind turbines and cannot be neglected.

For the cases with irregular waves and constant wind, non-linear hydrodynamic effects present an important influence on the low-frequency platform dynamics in both surge and pitch. In this region, the numerical simulations using a linear hydrodynamic model underestimate the experimental response. When non-linear hydrodynamic effects are added to the computations by means of the full QTFs, the numerical predictions approach the experiments for low frequencies, but the response is still underestimated. Around the wave peak frequency, the response is dominated by linear hydrodynamics, and simulations agree well with the experiments independently of the hydrodynamic model chosen.

The inclusion of turbulent wind using SiL in cases with irregular waves introduces a low-frequency excitation that can dominate the platform motions at this region, depending on the wind speed. In particular, for mean wind speeds close to the rated (where the rotor thrust is the highest), the differences introduced by non-linear hydrodynamics are hidden. In this case, the agreement between experiments and computations is very good in all the range of frequencies, independently of the model to compute the hydrodynamics. However, for turbulent winds with mean speeds producing a lower rotor thrust, the non-linear hydrodynamics play a role on the low-frequency surge motion. In these cases, non-linear hydrodynamics must be included in numerical models to better capture the floating platform dynamics. Nevertheless, even with non-linear hydrodynamics included in the simulation model, the surge low-frequency response of the platform can be underestimated in comparison with experiments.

The cases with turbulent wind and irregular waves show a good agreement between computations and experiments in all the range of frequencies. The comparison of numerical and measured decay tests also indicates a good integration of the rotor aerodynamic damping in the scaled tests. In consequence, the SiL method has performed successfully during the tests to integrate the scaled coupled aerodynamics based on a BEM real-time computation that included the control strategy, the aerodynamic damping, and the wind turbulence. However, it has to be kept in mind that the SiL method includes the rotor thrust based on a numerical model and a specific experimental validation of the rotor aerodynamics, for instance, in a wind tunnel, may be required.

Hybrid testing methods are a promising methodology to resolving the scaling conflict between the aerodynamics and the hydrodynamics in wave tank tests. Future work is planned to improve the method by including effects such as the gyroscopic or aerodynamic moments and by further validating the SiL method for other platform concepts.

ACKNOWLEDGEMENTS

The tests leading to these results have received support from MARINET, a European Community Research Infrastructure Action under the FP7 "Capacities" Specific Programme with grant agreement number 262552. Part of this work has been funded by the European Community's FP7 INNWIND.EU project, under grant agreement number 308974. The test campaign was a joint effort of different participants in the Task 4.2 of the INNWIND.EU project. In particular, we want to thank Frank Lemmer and Florian Amann, from the University of Stuttgart, for building the scaled model of the platform and verifying the physical properties. We also thank Filippo Campagnolo, from the Technical University of Munich, for providing the specifications of the tower where we integrated the ducted fan in the scaled model. We thank Jean Marc Rousset and Sylvain Bourdier, from the École Centrale de Nantes, for their assistance during the execution of the tests. We are very grateful to Amy Robertson, from NREL, for providing the QTF files for the non-linear hydrodynamic model of the OC4 DeepCwind platform.

ORCID

José Azcona https://orcid.org/0000-0003-0895-1049

REFERENCES

1. Bredmose H, Larsen SE, Matha D, Rettenmeier A, Marino E, Saettran L. D2.4: collation of offshore wind-wave dynamics. tech. rep., MARINET; 2012.
2. Azcona J, Bouchotrouch F, González M, Garciandía J, Munduate X, Kelberlau F, Nygaard T. Aerodynamic thrust modelling in wave tank tests of offshore floating wind turbines using a ducted fan. *J Phys Conf Ser*. 2014;524:012089. https://doi.org/110.1088/1742-6596/524/1/012089
3. Koch C, Lemmer F, Borisade F, Matha D, Cheng PW. Validation of INNWIND.EU scaled model tests of a semisubmersible floating wind turbine. In: Proceedings of the Twenty-sixth International Conference on Offshore and Polar Engineering; 2016; Rhodes, Greece.
4. Roddier D, Cermelli C, Aubault A, Weinstein A. Windfloat: a floating foundation for offshore wind turbines. *J Renewable Sustain Energy*. 2010;2:033104.
5. Chabaud V, Steen S, Skjetne R. Real time hybrid testing of marine structures: challenges and strategies. In: ASME 32nd International Conference on Ocean, Offshore and Arctic Engineering; 2013; Nantes, France:V005T06A021-V005T06A021.
6. Hall M, Moreno J, Thiagarajan K. Performance specifications for real-time hybrid testing of 1:50 scale floating wind turbine models. In: ASME 33rd International Conference on Ocean, Offshore and Arctic Engineering; 2014; San Francisco, CA, USA:V09BT09A047-V09BT09A047.
7. Bachynski E, Chavaud V, Sauder T. Real-time hybrid model testing of floating wind turbines: sensitivity to limited actuation. In: 12th Deep Sea Offshore Wind R&D Conference, EERA DeepWind; 2015; Trondheim, Norway.
8. Hall M, Goupee A. Validation of a hybrid modeling approach to floating wind turbines basin testing. *Wind Energy*. 2018;21(2):1-18.
9. Kanner S, Yeung RW, Koukina E. Hybrid testing of model scale floating wind turbines using autonomous actuation and control. In: OCEANS 2016 MTS/IEEE; 2016; Monterey, CA, USA:1-6.
10. Hall M, Goupee A, Jonkman J. Development of performance specifications for hybrid modeling of floating wind turbines in wave basin tests. *J Ocean Eng Marine Energy*. 2018;4(1):1-23.
11. Müller K, Sandner F, Bredmose H, Azcona J, Manjock A, Pereira R. Improved tank test procedures for scaled floating offshore. In: International Wind Engineering Conference; 2014; Hannover, Germany.
12. Bayati I, Jonkman J, Robertson A, Platt A. The effects of second-order hydrodynamics on a semisubmersible floating offshore wind turbine. *J Phys Conf Ser*. 2014;524:012094. https://doi.org/110.1088/1742-6596/524/1/012094
13. Duarte T, Sarmento A, Jonkman J. Effects of second-order hydrodynamic forces on floating offshore wind turbines. In: Proceedings of the 32nd ASME Wind Energy Symposium; 2014; National Harbor, Maryland, USA:0361.
14. Coulling A, Goupee A, Robertson A, Jonkman J. Importance of second-order difference-frequency wave-diffraction forces in the validation of a fast semi-submersible floating wind turbine model. In: ASME 32nd International Conference on Ocean, Offshore and Arctic Engineering; 2013; Nantes, France:V008T09A019-V008T09A019.
15. Goupee AJ, Koo BJ, Lambrakos KF, Kimball RW. Model tests for three floating wind turbine concepts. In: Offshore Technology Conference; 2012; Houston, TX, USA.
16. Thys M, Chabaud V, Sauder T, Eliassen L, Sæther LO, Øyvind BM. Real-time hybrid model testing of a semi-submersible 10MW floating wind turbine and advances in the test method. In: ASME 2018 1st International Offshore Wind Technical Conference; 2018; San Francisco, California, USA:V001T01A013-V001T01A013.
17. Robertson A, Jonkman J, Masciola M, Hong H, Goupee A, Coulling A, Luan C. Definition of the semisubmersible floating system for phase II of OC4. Technical Report NREL/TP-5000-60601, Boulder, CO, USA, NREL; 2014.

18. Jonkman J, Butterfield JS, Musial W, Scott G. Definition of a 5-MW reference wind turbine for offshore system development. Technical Report NREL/TP-500-38060, Boulder, CO, USA, NREL; 2009.
19. Jonkman J. Dynamics modeling and loads analysis of an offshore floating wind turbine. *PhD Dissertation*. Boulder, CO, USA: University of Colorado; 2007.
20. Jonkman BJ. TurbSim user's guide: version 1.50. Technical Report NREL/TP-500-46198, Boulder, CO, USA, NREL; 2009.
21. WAMIT, Inc. Massachusetts, USA. WAMIT user manual.
22. Hall M. *Moordyn User's Guide*. ME, USA; Department of Mechanical Engineering, University of Maine; 2015.
23. Det Norsk Veritas. *Offshore Standard DNV-OS-E301 Position Mooring*. Høvik, Norway: DNV; 2010.
24. Bureau Veritas. Classification of mooring systems for permanent offshore units. Courbevoie (France): Bureau Veritas, NR 493 R02 E; 2002.

How to cite this article: Azcona J, Bouchotrouch F, Vittori F. Low-frequency dynamics of a floating wind turbine in wave tank–scaled experiments with SiL hybrid method. *Wind Energy*. 2019;1–12. https://doi.org/10.1002/we.2377